symmetry

MDPI

Article

Density Functional Theory Study of Substitution Effects on the Second-Order Nonlinear Optical Properties of Lindquist-Type Organo-Imido Polyoxometalates

Emna Rtibi [1,2] and Benoit Champagne [2,*]

[1] Laboratory of Materials Molecules and Applications, Preparatory Institute for Scientific and Technical Studies, Carthage University, B.P. 51 La Marsa, Tunis 2075, Tunisia; emna.rtibi@unamur.be
[2] Laboratory of Theoretical Chemistry, Unit of Theoretical and Structural Physical Chemistry, Namur Institute of Structured Matter, University of Namur, Rue de Bruxelles, 61, 5000 Namur, Belgium
* Correspondence: benoit.champagne@unamur.be; Tel.: +32-081-724-554

Abstract: Density functional theory and time-dependent density functional theory have been enacted to investigate the effects of donor and acceptor on the first hyperpolarizability of Lindquist-type organo-imido polyoxometalates (POMs). These calculations employ a range-separated hybrid exchange-correlation functional (ωB97X-D), account for solvent effects using the implicit polarizable continuum model, and analyze the first hyperpolarizabilities by using the two-state approximation. They highlight the beneficial role of strong donors as well as of π-conjugated spacers (CH=CH rather than C≡C) on the first hyperpolarizabilities. Analysis based on the unit sphere representation confirms the one-dimensional push-pull π-conjugated character of the POMs substituted by donor groups and the corresponding value of the depolarization ratios close to 5. Furthermore, the use of the two-state approximation is demonstrated to be suitable for explaining the origin of the variations of the first hyperpolarizabilities as a function of the characteristics of a unique low-energy charge-transfer excited state and to attribute most of the first hyperpolarizability changes to the difference of dipole moment between the ground and that charge-transfer excited state.

Keywords: polyoxometalates; donor/acceptor substituents; first hyperpolarizability; (time-dependent) DFT

Citation: Rtibi, E.; Champagne, B. Density Functional Theory Study of Substitution Effects on the Second-Order Nonlinear Optical Properties of Lindquist-Type Organo-Imido Polyoxometalates. *Symmetry* **2021**, *13*, 1636. https://doi.org/10.3390/sym13091636

Academic Editors: Christophe Humbert and Thomas Noblet

Received: 14 July 2021
Accepted: 24 August 2021
Published: 6 September 2021

1. Introduction

Polyoxometalates (POMs) are nanomolecular metal-oxides made of metal atoms (M) from groups VB (often, V) and VIB (often Mo or W) in a high oxidation state. These anionic nanoclusters are built from MO_x^{y-} oxyanion polyhedra linked together by shared O atoms. Much is known about their redox properties, leading to interesting catalytic activities [1], while they also found applications in life sciences [2]. Moreover, recent experimental investigations have demonstrated that POM units can be combined with organic moieties, leading to hybrid organic-inorganic compounds that exhibit nonlinear optical (NLO) properties [3–7]. Though reference [6] deals with third-order NLO effects, the other investigations as well as the current contribution focus on the second-order NLO effects and, more precisely, on second harmonic generation (SHG). These experimental studies [3–5,7] extended the field of organic and organometallic compounds, which can present large second-order NLO responses combined with short response times [8–25]. In particular, refs. [3,4] demonstrated that POMs may provide a new generation of high performance, high transparency, and potentially redox-switchable NLO materials. In the case of Lindqvist-type organo-imido-substituted hexamolybdates bearing π-conjugated ligands, these investigations demonstrated that the polyanion clusters act as electron acceptors because the first hyperpolarizability (β), which characterizes the SHG response at the molecular scale, is enhanced when these organic linkers are substituted by electron

donors, in other words, when they present a strong non-centrosymmetry. These experimental characterizations have been carried out using the hyper-Rayleigh scattering (HRS) technique [26]. Though these interpretations were in contradiction with previous quantum chemical calculations [27,28], a recent contribution by the authors [29] showed that the polyanions of these Lindqvist-type POMs play the role of electron acceptor and that the use of an inappropriate density functional theory (DFT) exchange-correlation functional (XCF) was responsible for the incorrect structure-property relationships in refs. [27,28]. In reference [29], a striking difference with respect to the previous theoretical studies results from the use of a range-separated hybrid XCF, known to describe reliably the hyperpolarizabilities. Indeed, (linear and) nonlinear electric-field-induced polarization effects, which determine the β responses, are intrinsically nonlocal and require the use of XCFs that contain nonlocal (Hartree-Fock) exchange [30]. On the contrary, local density approximation (LDA) and generalized-gradient approximation (GGA) suffer from shortsightedness to the electric field perturbations, as previously demonstrated and analyzed [31–33].

Following reference [4], 11 hexamolybdate compounds (labeled **0–10**) have been selected in reference [29] and a detailed quantum chemical investigation has been enacted. Besides the selection of reliable methods to predict their geometrical structures, linear and nonlinear optical responses, that work provided an interpretation of the second-order NLO responses in agreement with the experimental data, bringing additional tools to deduce structure-property relationships and to support the design of new POM derivatives with large NLO responses. In this work, we extend our previous investigation by addressing one aspect of the structure-NLO property relationships in Lindqvist-type POMs: the modulation of the donor/acceptor character of the organic linker either by changing the substituent on the terminal phenyl ring or by changing the π-conjugated character by replacing the CC triple bond by a CC double bond (Figure 1).

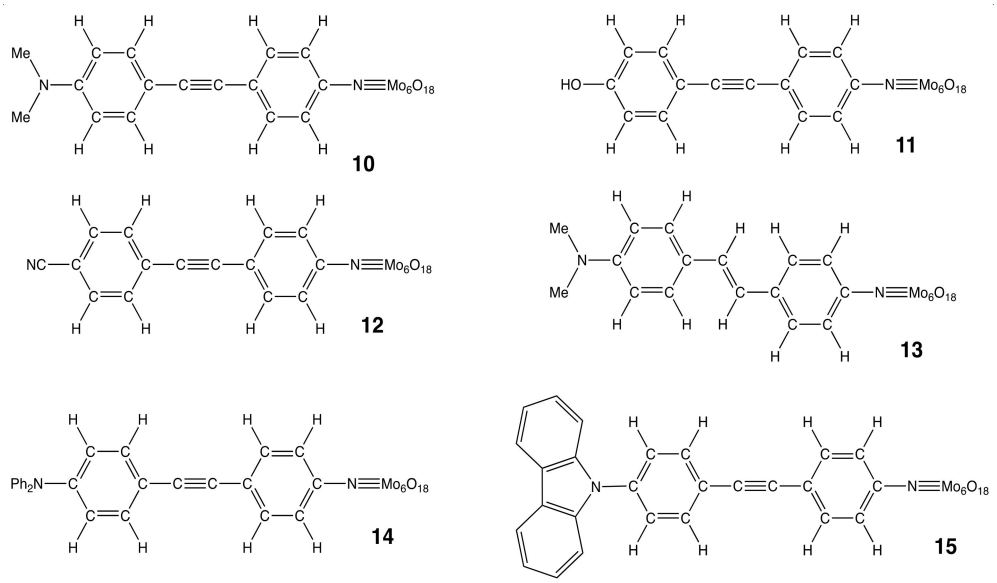

Figure 1. Structure of POM derivatives **10**–**15**. POMs **0–10** have been studied in our previous work (reference [29]), and a consistent notation has been adopted for easing the discussion.

The first point is tackled by starting from compound **10** and by changing its dimethylamino substituent, either by small groups, a hydroxyl substituent (**11**), or a cyano one (**12**). This will further confirm the contrasted role of acceptor and donor groups (CN versus OH and NMe_2). Then, the comparison between **10** and **13** aims at comparing the role of the linker, containing an ethynyl (**10**) or an ethenyl (**13**) spacer. Finally, based on reference [5], other donor groups are considered. These are bulkier than in **10**, a diphenylamino (**14**) or a carbazole (**15**) substituent.

2. Computational Methods

DFT and TDDFT calculations were carried out using the Gaussian16 package [34]. Geometry optimizations were performed using ωB97X-D XCF [35], which includes 100% of long-range exact exchange, a small fraction (about 22%) of short-range exact exchange, a modified B97 XCF for short-range interaction, the B97 correlation density functional [36] and empirical atom−atom London dispersion corrections. The default range-separating parameter ω = 0.2 Bohr^{-1} was used. The atomic basis set consists of 6-311+G(d,p) for C, H, N, O, and LANL2TZ for the Mo atoms. The reliability of this ωB97X-D/6-311+G(d,p)/LANL2TZ method for the geometry optimization of POM derivatives was demonstrated in comparison with other XC functionals in our previous work [29] and was confirmed here by comparison with experimental data from reference [3]. To better describe the impact of the solvent effects, geometry optimizations were performed in solution using the integral equation formalism (IEF) of the polarizable continuum model (PCM) (IEF-PCM), which represents the solvent by a dielectric continuum characterized by its dielectric permittivity (ε) [37]. Using the optimized geometries, the SHG β tensor components were calculated employing the time-dependent density functional theory (TDDFT) method [38,39] with the ωB97X-D XC functional, the 6-311G(d)/LanL2TZ basis set, and the IEF-PCM scheme to account for solvent effects. Both static and dynamic responses were evaluated for an incident wavelength of 1064 nm. Computing β has always been a challenge, in particular, for large compounds and for compounds having donor and/or acceptor substituents because of the intrinsic nonlocal nature of the response. ωB97X-D falls in a new class of DFT functional known as range-separated functionals, which are capable of capturing both short-range and long-range interactions.

To allow comparisons with the experiment, the HRS first hyperpolarizabilities, $\beta_{HRS}(-2\omega;\omega,\omega)$, were evaluated from the β tensor components. These are reported as well as the depolarization ratios (DR), which reflects the NLOphore shape. Full expressions for $\beta_{HRS}(-2\omega;\omega,\omega)$ and DR are available from refs. [40,41]. In the case of one-dimensional push-pull π-conjugated systems, the β tensor is dominated by a single diagonal component, β_{zzz}, where z is the charge-transfer axis. In that case, there is a simple relationship between β_{HRS} and that component [4]:

$$\beta_{zzz} = \sqrt{35/6}\beta_{HRS} \tag{1}$$

To describe the first hyperpolarizability, the unit sphere representation (USR) was adopted [42]. It consists (i) in evaluating an effective induced dipole:

$$\vec{\mu}_{ind} = \overleftrightarrow{\beta} : \vec{E}^{2}(\theta,\phi) \tag{2}$$

where $\overleftrightarrow{\beta}$ is the first hyperpolarizability tensor and $\vec{E}(\theta,\phi)$ is a unit vector of the electric field, of which the polarization is defined in spherical coordinates by the θ and ϕ angles, and (ii) then in representing the induced dipoles on a sphere centered at the molecule center of mass. The interpretation of the β values can further be performed by resorting to perturbation theory, where β is expressed under the form of a summation over the excited states (SOS) [43,44]. In particular, the reliability of the two-state approximation (TSA) has been demonstrated for push-pull π-conjugated systems [45]. In that scheme, the β response is dominated by a single low-energy charge-transfer excited state and, for the diagonal component along the charge-transfer axis, $\beta_{zzz} = \beta$:

$$\beta = 6\frac{\Delta\mu_{ge}\mu_{ge}^{2}}{\Delta E_{ge}^{2}} = 9\, f_{ge}\,\frac{\Delta\mu_{ge}}{\Delta E_{ge}^{3}} \tag{3}$$

where $\Delta E_{ge} = E_e - E_g$, the excitation energy from the ground state g to the excited state e, is the lowest-energy dipole-allowed excited state, $\Delta\mu_{ge} = \mu_e - \mu_g$ is the corresponding

difference in dipole moment, and μ_{ge} is the transition dipole moment, related to the oscillator strength f_{ge} of the excitation:

$$f_{ge} = \frac{2}{3}\Delta E_{ge}\mu_{ge}^2 \quad (4)$$

3. Results and Discussion

3.1. Ground State Equilibrium Geometries

Selected ground state equilibrium geometrical parameters of compounds **10–15**, which have been optimized with the IEF-PCM/ωB97X-D/6-311G*/LanL2TZ method, are displayed in Table 1 and compared with the experimental results from X-ray diffraction (XRD) (**10**, **14,** and **15**).

Table 1. Selected equilibrium bond lengths (in Å) and valence angles (deg.) of POMs derivatives as obtained at the IEF-PCM/ωB97X-D/6-311G*/LanL2TZ level in comparison with experimental results from X-ray diffraction [1,2].

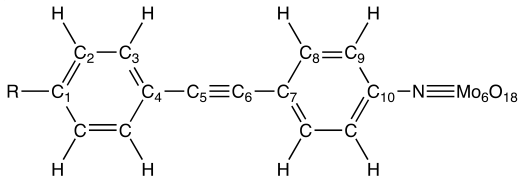

Compounds	**10**		**11**	**12**	**13**	**14**		**15**	
Method	**DFT [29]**	**XRD [4]**	**DFT**	**DFT**	**DFT**	**DFT**	**XRD [5]**	**DFT [3]**	**XRD [5]**
R-C_1	1.367	1.368	1.352	1.432	1.371	1.403	1.385	1.413	1.447
C_1-C_2	1.413	1.411	1.395	1.398	1.412	1.401	1.406	1.395	1.390
C_2-C_3	1.382	1.385	1.386	1.383	1.382	1.383	1.388	1.385	1.392
C_3-C_4	1.400	1.403	1.401	1.401	1.401	1.401	1.395	1.400	1.388
C_4-C_5	1.424	1.430	1.427	1.427	1.462	1.426	1.448	1.428	1.474
C_5-C_6	1.208	1.208	1.207	1.206	1.342	1.207	1.198	1.207	1.210
C_6-C_7	1.425	1.433	1.426	1.426	1.465	1.426	1.438	1.427	1.489
C_7-C_8	1.403	1.385	1.402	1.402	1.404	1.403	1.400	1.402	1.389
C_8-C_9	1.384	1.384	1.382	1.383	1.382	1.383	1.362	1.383	1.391
C_9-C_{10}	1.397	1.391	1.400	1.400	1.400	1.400	1.417	1.402	1.390
C_{10}-N	1.373	1.395	1.375	1.374	1.374	1.374	1.382	1.378	1.373
N-Mo	1.727	1.737	1.729	1.730	1.727	1.728	1.755[5]	1.734	1.750
Mo-O	1.980	1.946	1.983	1.981	1.984	1.981	1.952	1.985	1.955
Mo-Mo	3.303	3.237	3.303	3.303	3.303	3.305	3.245	3.301	3.230
C_{10}-N-Mo	169.6	168.3	170.0	169.9	174.9	176.7	172.3	168.3	160.6
BLA [4]	0.024	0.023	0.012	0.016	0.024	0.018	0.012	0.012	−0.003

[1] When they are several equivalent atoms in the molecule or more than one molecule in the unit cell, the reported values are averages. [2] The C_5 and C_6 atoms of the general structure correspond either to ethenyl or ethynyl C atoms. [3] In compound **15**, the calculated torsion angle between the carbazole and the attached phenyl ring amounts to 55.6° while in the crystal it attains 69.9°. [4] BLA is defined as $\frac{1}{2}$[2 d (C_2-C_3)—d (C_1-C_2)—d (C_3-C_4)]. [5] The average is not reported here since the equivalent bond length for the other molecule of the unit cell amounts to 2.038 Å, which is beyond what could be expected for such an N-Mo bond.

The agreement is globally suitable, though the medium effects are different, i.e., the calculations do not account for crystal packing effects but for an isotropic dielectric medium (which is consistent with the calculations of the NLO responses, compared to measurements carried out in solution). Differences in bond lengths are generally of the order of 0.02 Å or less. For the C_{10}-N-Mo valence angle, the difference can attain 4–8°, which is attributed to the crystal environment.

Comparing **10** and **13**, besides the ethenyl versus ethynyl linker, the differences of geometry are very small (0.005 Å or less on the bond lengths and the same BLA value). This is consistent with their similar charge distributions in the ground state (vide infra). Then, comparing the optimized geometries of compounds with a CC triple bond as a

spacer, differences in BLA are obvious. In the case of **10**, the BLA amounts to 0.024 Å and decreases to 0.018 Å in **14** (R = NPh_2) and 0.012 Å in **15** (R = carbazole). In fact, the BLA is a probe of the donor or acceptor strength of the substituent. When the substituent is a H atom (compound **0** from reference [29]), the BLA reduces to 0.008 Å while with the dimethylamino group (**10**), which is a strong donor, the quinoid character of the ring increases, and the BLA increases to 0.024 Å. So, on the basis of the BLA, the donor character decreases in the order NMe_2 > NPh_2 > carbazole. When R = OH (**11**), the BLA also amounts to 0.012 Å. When the substituent is a cyano group (**12**), it is slightly larger (0.016 Å), highlighting the acceptor character of that group. Note that in the case of **15**, the BLA is similar to that found in compounds **4** and **8** of reference [29], which involve a pyrrolyl substituent. Indeed, such as the pyrrolyl substituent, the carbazole of **15** is tilted (by 56°) with respect to the plane of the attached phenyl ring, reducing the donor character of the N atom. Moreover, the phenyl rings of the NPh_2 substituent in **14** are also tilted with respect to the phenyl of the π-conjugated linker, but the tilt angle is smaller than in **15** and goes down to 33°.

These BLA variations and the subsequent interpretation of the donor strengths are corroborated by the C_1-N bond lengths, which increase in the order NMe_2 < NPh_2 < carbazole (both from XRD data and from calculations). The substituent effects on the other geometrical parameters are much smaller because these units (CC triple bond, the other phenyl ring, and the POM moiety) are farther away.

3.2. Natural Population Analysis (NPA) Charge Distributions

Natural population analysis (NPA) was carried out for the different segments of the POMs, as defined in Table 2. The NPA charge on the POM moiety is always close to −1.9 e, while for the linking N atom (**E** moiety) and the nearby phenyl ring (**D** moiety), they amount to −0.3 e and 0.2 e. These sum up to −2 e, which is the global anion charge. The ethynyl/ethenyl spacer can be considered neutral, with negligible impact on the substituent. Thus, the global charge of the **A** and **B** units is also zero, and the differences refer to the donor/acceptor strengths. In the case of **10**, both **A** and **B** bear a quasi-zero charge. When replacing the NMe_2 substituent with NPh_2 and then a carbazole, the substituent becomes more negative. This can be explained by the fact that its donor (mesomer) character does not compensate anymore for the acceptor (inductive) effect of the N atom. In the case of **11**, the donor character of the hydroxyl group is smaller than that of the NMe_2 in **10,** while the acceptor character of the cyano group appears small, with a charge of −0.04 e.

Table 2. Natural Population Analysis charge distributions (in e) in the **A**–**F** moieties of compounds **10–15**, as obtained from calculations performed at the IEF-PCM/ωB97X-D/6-311G*/LanL2TZ level of approximation. The **A**–**F** moieties are defined in the scheme below.

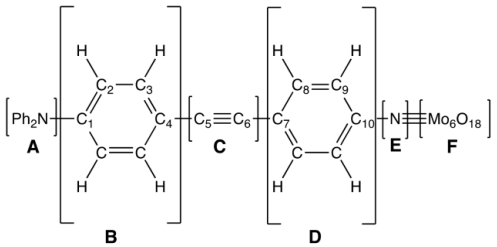

Compounds	A	B	C	D	E	F
10 (**A** = −NMe_2, **C** = C≡C)	0.01	0.04	−0.01	0.19	−0.30	−1.93
11 (**A** = −OH, **C** = C≡C)	−0.19	0.22	−0.01	0.20	−0.30	−1.91
12 (**A** = −CN, **C** = C≡C)	−0.04	0.01	0.02	0.21	−0.31	−1.89
13 (**A** = NMe_2, **C** = CH=CH)	0.00	0.04	0.02	0.18	−0.29	−1.95
14 (**A** = −NPh_2, **C** = C≡C)	−0.12	0.14	0.00	0.20	−0.30	−1.92
15 (**A** = −Carb., **C** = C≡C)	−0.21	0.21	0.01	0.21	−0.31	−1.91

3.3. First Hyperpolarizabilities

The first hyperpolarizabilities of compounds 10−15 are listed in Table 3. Besides the β_{HRS} values and their depolarization ratios, the $\beta_{zzz} = \sqrt{35/6}\beta_{HRS}$ values are reported to allow straightforward comparisons with the experiment. To a suitable extent, variations of the β values are consistent with the BLA values: a large BLA leads to a large β value. This is substantiated by the relative β values of the compounds bearing an amino substituent: β(**10**, NMe_2) > β(**14**, NPh_2) > β(**15**, carbazole). On this basis, the dimethylamino group is a better donor than the diphenylamino one, both being stronger than carbazole. The weaker donor character of carbazole can be associated with its steric interactions with the phenyl ring, leading to a twist by about 56° and a subsequent reduction in π-conjugation. The intermediate value of **14** is then associated with the twist of the phenyl rings (33°). This BLA-β relationship is also verified by the differences between compounds **11** (R = OH) and **10** (R = NMe_2). Nevertheless, the BLA is not the only criterion to take into account. So, compound **12** bearing a cyano group has a much smaller β value than reference compound **10** in comparison to compound **11**. This is attributed to the acceptor character of the cyano substituent, which, although it affects the BLA of the phenyl ring, is poorly conjugated with the POM acceptor moiety (vide infra). In addition, compounds **10** and **13** have similar BLA values, but the β value of compound **13** is 21% (41%) larger than that of compound **10** in the static limit (at 1064 nm). This is explained by the nature of the spacer between the phenyl rings: a single-double-single bond pattern enables better the propagation of the donor effect than a single-triple-single bond pattern.

Table 3. HRS first hyperpolarizabilities (in 10^3 au) of the POM derivatives as calculated at the IEF-PCM(solvent = acetonitrile)/TDDFT/ωB97X-D/6-311G*/LanL2TZ level in comparison with experimental data from reference [5]. Depolarization ratios are given in parentheses. Columns 4,5 report the β_{zzz} values (in 10^{-30} esu, B convention, i.e., the values are divided by two with respect to the T convention values) while column 6 reports the corresponding β_{zzz} experimental values.

Compounds	β_{HRS}		β_{zzz}		β_{zzz}, **Exp.**
	λ=∞	λ = **1064 nm**	λ=∞	λ = **1064 nm**	λ = **1064 nm**
10	20.8 (4.75)	42.4 (4.94)	217	443	440 ± 55
11	11.3 (4.75)	19.2 (4.94)	118	200	/
12	3.2 (4.55)	5.4 (4.92)	34	56	/
13	25.2 (4.77)	58.5 (4.96)	263	611	/
14	17.0 (4.49)	36.6 (4.52)	177	382	590 ± 20
15	8.8 (4.37)	16.6 (4.50)	92	173	150 ±36

The DR values are generally close to 5, which is the typical value for one-dimensional push-pull π-conjugated systems, which whom the β tensor is dominated by a single diagonal component (along the charge-transfer axis, called here β_{zzz}). This ratio gets also closer to 5 when going from the static value to the response at 1064 nm. The DR is also slightly smaller for compounds **14** and **15**, which is attributed to the more extended nature of the donor substituents. The USRs of the β tensor further describe the second-order responses of these POM derivatives (Figure 2). All USRs highlight the non-centrosymmetry of the second-order NLO response as well as the strong one-dimensional push-pull character of these compounds. The arrows go from the acceptor (POM moiety) to the donor groups. Their lengths are proportional to the amplitude of the β response in a given direction. Note that in the case of the cyano group, the arrows are much smaller but still oriented in the same direction, which attributes to the POM a stronger acceptor character than to the cyano group.

Comparisons to the experiment confirm that the carbazole group is the weakest donor among the three amino substituents because the β_{HRS} response is substantially smaller for compound **15** than for **10** and **14**. On the other hand, there is an inversion between the relative values of compounds **10** and **15**. First, the quantitative agreement between

theory and experiment is very suitable for **10,** but for **15**, calculations predict a decrease by 14%, while experiments show an increase by 34% with respect to **10**. This difference might result from the combination of the limitations of the method of calculation (the XCF and the treatment of the solvent are approximate), together with the experimental error bars.

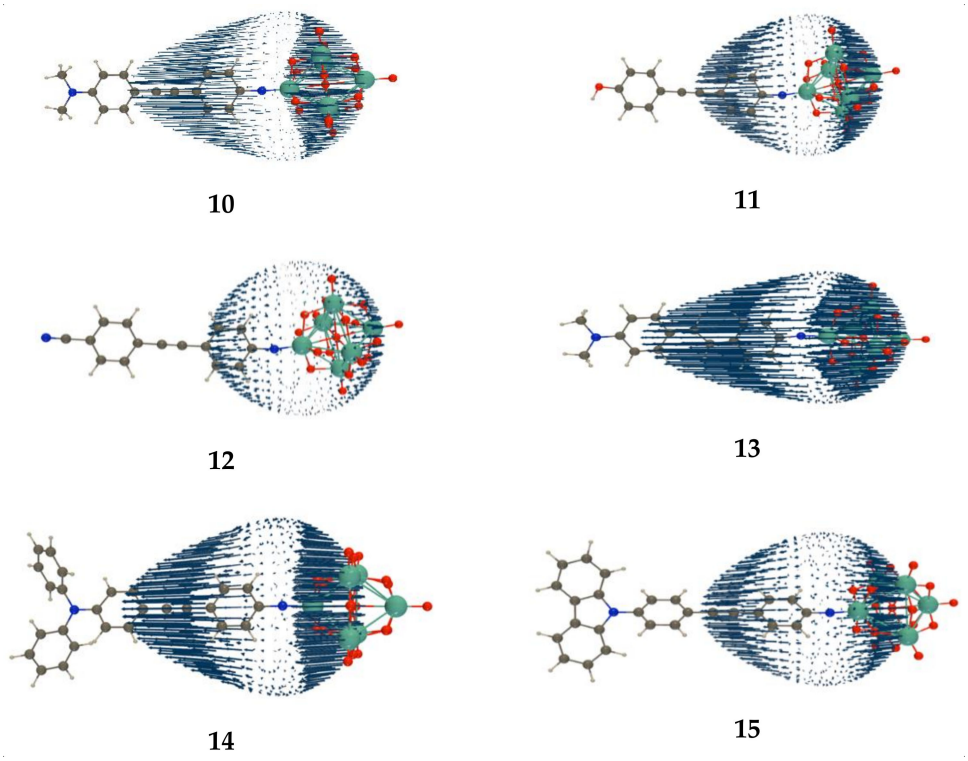

Figure 2. Unit sphere representation of the static first hyperpolarizability tensor of compounds **10–15**, as calculated at the TDDFT/ωB97X-D level of approximation (USR factor of 0.0001).

3.4. UV-Absorption Spectra and Interpretation of the β Values

The UV/visible absorption spectra of POMs **10–15** were simulated at the TDDFT level and are drawn in Figure 3. At large wavelengths (330–450 nm), they are dominated by a single transition, which corresponds to the second excited state. The characteristics of that state are listed in Table 4. Besides the excitation energy and oscillator strength, the charge-transfer distance (d_{CT}) and amplitude (q_{CT}), together with the change of dipole moment upon excitation ($\Delta\mu_{CT}$) are listed.

Starting from **10**, the lowest excitation energy band is blue-shifted by ~0.2 eV for compounds **11** and **12** while it is red-shifted by almost 0.2 eV for compound **13**, characterized by a better π-conjugated spacer between the phenyl rings. In the case of the amino-like substituents, comparison with the experiment is possible. Their calculated vertical excitation energies are systematically larger than the photon energies corresponding to the maximum of absorption (by 0.22–0.31 eV). This is consistent with the difference of nature between these two quantities and, subsequently, the fact that the maximum absorption is lowered in energy by about 0.2 eV with respect to the vertical excitation energy, as calculated recently for fluorescent protein chromophores [46]. Among these three amino-like compounds, POM **10** presents the smallest calculated (experimental) excitation energy, 2.98 eV. It is blue-shifted by 0.04 eV (experimentally, 0.04 eV as well) when the substituent is NPh_2 (**14**) and by 0.17 eV (experimentally, 0.26 eV) when it is a carbazole (**15**). Among these, **14** presents the largest calculated oscillator strength (f) and experimental extinction coefficient. **10** and **13**, which differ by the π-spacer, present similar oscillator strengths, which are larger than those of POMs **11** and **12**.

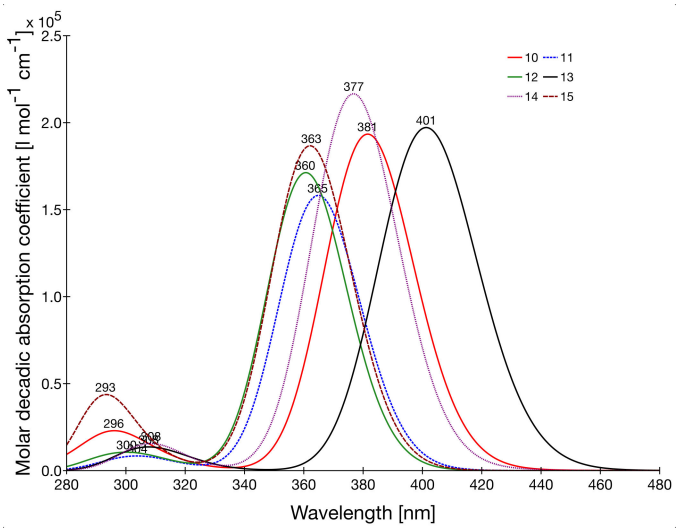

Figure 3. UV/visible absorption spectra of compounds **10–15** as obtained at the IEF-PCM/TDDFT/ωB97X-D/6-311G*/LanL2TZ level of approximation. Each transition is described by a Gaussian having an HWHM = 0.3 eV.

Table 4. UV/visible spectra characteristics of compounds **10–15** as determined at the IEF-PCM(solvent = acetonitrile)/TDDFT/ωB97X-D/6-311G*/LanL2TZ level of approximation. The β_{HRS} and β_{HRS} quantities have been evaluated using the two-state approximation (in 10^3 a.u.) and the CPKS β_{HRS} values are also given for comparison.

POMs	ΔE (eV) (λ, nm) [Root]	ΔE (Exp.)	f	d_{CT} (Å)	q_{CT} (e)	$\Delta\mu$ (D)	$\beta_{zzz}^{TSA}=9\frac{f\,\Delta\mu}{\Delta E^3}$	β_{HRS}^{TSA}	β_{HRS}^{CPKS}
10	3.25 (382) [2]	2.94 [5]	2.15	4.78	0.66	15.2	67.9	28.1	20.8
11	3.40 (365) [2]	-	1.76	3.56	0.57	9.8	31.1	12.9	11.3
12	3.44 (361) [2]	-	1.90	1.97	0.50	4.7	15.7	6.5	3.2
13	3.09 (401) [2]	-	2.19	4.83	0.66	15.4	81.6	33.8	25.2
14	3.29 (377) [2]	2.98 [5]	2.41	4.38	0.62	13.0	62.6	25.9	17.0
15	3.42 (362) [2]	3.20 [5]	2.08	3.08	0.54	8.0	29.6	12.2	8.8

For the dominant electronic excitation, the change of electron density, $\Delta\rho\left(\vec{r}\right) = \rho_{excited}\left(\vec{r}\right) - \rho_{ground\ state}\left(\vec{r}\right)$, was calculated (Figure 4). The patterns are similar: they highlight the acceptor character of the POM moiety and the donor character of the terminal organic moiety. Moreover, their extents differ among the compounds. For **12**, the $\Delta\rho$ hardly spreads over the phenyl ring that bears the acceptor cyano group. For the other compounds, the terminal phenyl ring is involved. For **15**, only the N atom of the carbazole takes part as donating moiety. The donating contribution of the amino groups is larger in **14** and even more in **10** and **13**. By integration of the volumes with positive or negative $\Delta\rho$, the changes of dipole moment upon excitation, $\Delta\mu$, were evaluated. Their ordering is opposite to the corresponding excitation energies: **13** < **10** < **14** < **11** < **15** < **12**. This change of dipole moment, which can be expressed as the product between a charge-transfer distance (d_{CT}) and the amount of charge transfer (q_{CT}), is dominated by the former. Indeed, the range of q_{CT} values is narrow, 0.50–0.66 e, while the range of d_{CT} values is much broader, from 1.97 Å in **12** to more than twice as much in **10**, **14**, and **15**.

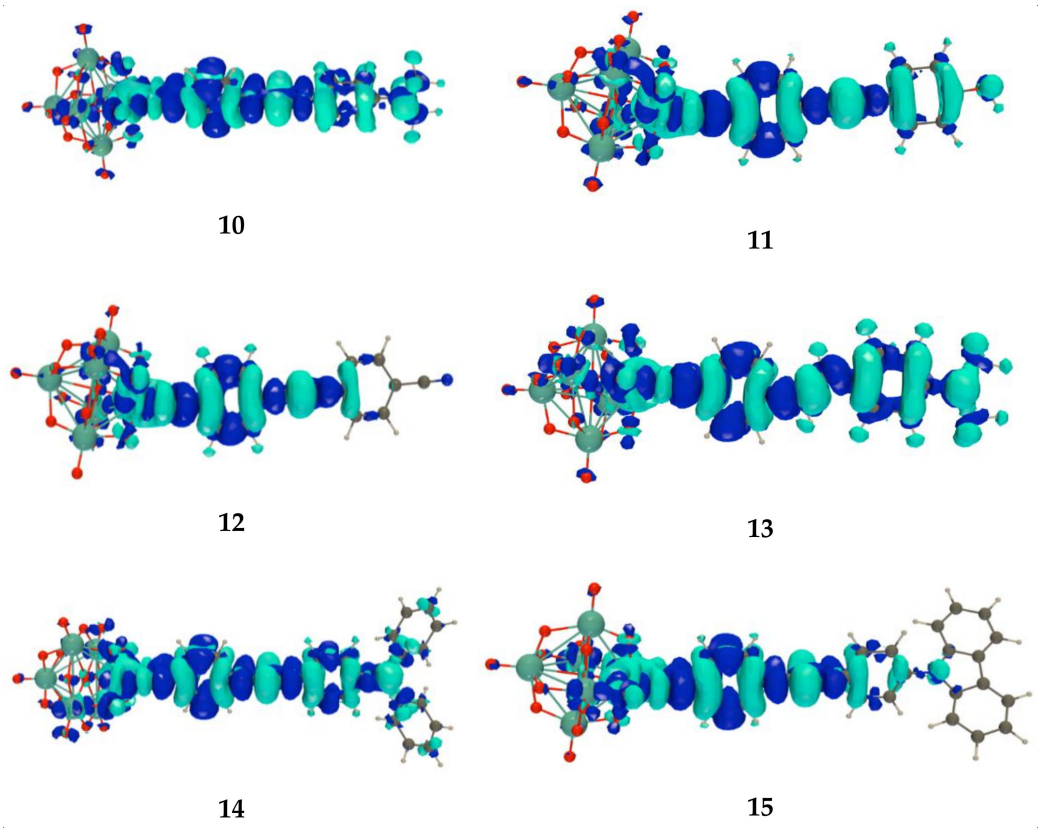

Figure 4. Excitation-induced electron density difference ($\Delta\rho\left(\vec{r}\right)$) as calculated for the key excited state of POMs **10–15** at the IEF-PCM/TDDFT/ωB97X-D/6-311G*/LanL2TZ level of approximation (iso-value = 0.0005 a.u.; light/dark blue corresponds to negative/positive $\Delta\rho\left(\vec{r}\right)$ so that the excitation-induced electron transfer goes from the light to the dark blue).

In the case of **10**, **14**, and **15**, these TDDFT/ωB97X-D UV/vis absorption characteristics are not straightforward to compare with those reported in reference [5], obtained at the TDDFT level with the SAOP (statistical average of orbital potential) XCF because their lowest excitation energy absorption bands result from more than one electronic transition with non-negligible oscillator strength, while in our case, there is only one transition. The comparison with the Stark spectroscopy data of reference [5] is also difficult for the same reason (more than one excited state) as well as owing to the specific experimental conditions (butyronitrile glasses at 77 K).

The linear optical properties were then employed to calculate the first hyperpolarizabilities within the TSA, [45] in fact the assumed dominant diagonal component of the β tensor in the direction of the CT axis, β_{zzz}^{TSA}, and from these the β_{HRS}^{TSA} values (Table 4). This assumption has been demonstrated to be valid because the DRs are close to the reference value of 5. A comparison between the TSA and CPKS static β_{zzz} values is provided in Figure 5. The agreement between the two sets of β_{zzz} values is excellent, with a correlation factor of 0.97. The slope of the least-squares fit linear relationship amounts to 1.31, indicating that the TSA overestimates, on average, the CPKS values by 31%. Such an overestimation of the TSA approach has been observed in other quantum chemistry investigations [47]. For our target compounds, the TSA is, therefore, a reliable model to explain the variations of β_{HRS} values and, the data of Table 4 points out that their variations are mostly governed by $\Delta\mu$ (and specifically, d_{CT}), then, on an equal foot, by the excitation energies and oscillator strengths (transition dipoles).

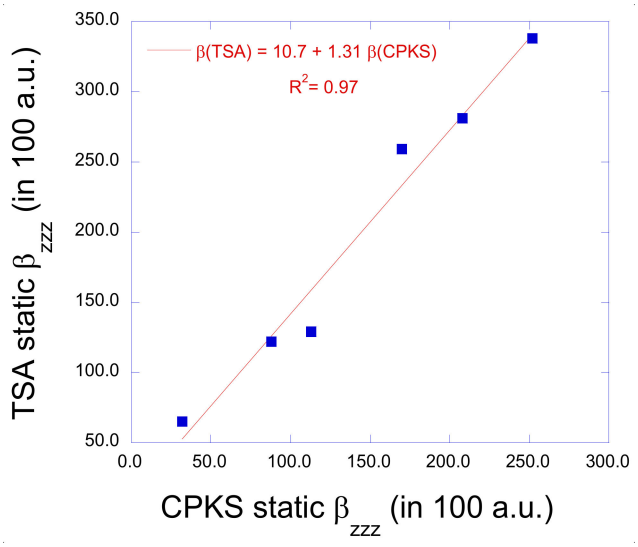

Figure 5. Comparison between static β_{zzz} values obtained within the two-state approximation and the full values calculated at the response TDDFT level (CPKS in the static limit). All β quantities have been obtained at the IEF-PCM/TDDFT/ωB97X-D/6-311G*/LanL2TZ level of approximation and are expressed in 10^2 a.u.

4. Conclusions and Outlook

Following reference [29], density functional theory and time-dependent calculations have been performed on an extended series of Lindquist-type organo-imido polyoxometalates derivatized with ligands bearing donor or acceptor groups to unravel the relationships between their structures and first hyperpolarizabilities. The electron acceptor character of the hexamolybdate moiety has been confirmed by these new quantum chemical analyses, highlighting that when associated with a donor substituent, its first hyperpolarizability increases, and stronger donor leads to larger first hyperpolarizabilities. By adopting a range-separated hybrid XC functional (ωB97X-D) and by describing solvent effects with the polarizable continuum model, a set of consistent data has been obtained: a stronger donor substituent on the terminal phenyl ring (i) increases its quinoid character (larger bond length alternation), (ii) augments the charge transfer between the substituent and that phenyl ring in the electronic ground state, (iii) decreases the excitation energy corresponding to the dominant low-energy excitation band, (iv) increases the oscillator strength, and (v) strongly enhances the excitation-induced change of dipole moment. In particular, in comparison to an ethynyl, the presence of an ethenyl π-spacer between the phenyl rings is favorable to achieve a large first hyperpolarizability. A larger first hyperpolarizability and corresponding consistent differences in the linear optical responses are also achieved in the case of a dimethylamino donor group, in comparison to a hydroxyl substituent, and even more in comparison to a cyano acceptor group.

Calculations have also enabled comparisons with recent experimental investigations [5], involving dimethylamino, diphenylamino, and carbazole moieties as donor groups. Calculations and experimental data highlight the weaker donor character of the carbazole moiety, which is attributed to the torsion angle between the carbazole and the attached phenyl ring, leading to a reduction in π-conjugation. On the other hand, calculations and experiments provide different conclusions on the comparison between POM bearing the dimethylamino or diphenylamino donor group. This difference is associated with the combination of the limitations of the method of calculation (the XCF and the treatment of the solvent are approximate) and of the experimental error bars.

Other structural effects of the POM on the first hyperpolarizability can be considered, such as the combination of two POM moieties with one organic linker, as proposed in reference [6], or the opposite, two organic ligands on one POM moiety. In both cases, the NLO performance of these Λ-shape compounds could be compared to those of their

push-pull one-dimensional derivatives. Another direction would be to consider POM containing two types of metal atoms, such as the combination of W and Mo atoms in reference [48].

Author Contributions: Conceptualization, B.C.; formal analysis, E.R. and B.C.; investigation, E.R.; writing—original draft preparation, E.R. and B.C.; writing—review and editing, B.C.; supervision, B.C.; project administration, B.C.; funding acquisition, B.C. Both authors have read and agreed to the published version of the manuscript.

Funding: This research was funded by the University of Namur, the FNRS-FRFC (Conventions No. GEQ U.G006.15, U.G018.19, and RW/GEQ2016), and the Walloon Region (Convention RW/GEQ2016).

Data Availability Statement: Data are stored on the computers of the HPC platform of UNamur.

Acknowledgments: The calculations were performed on the computers of the Consortium des Équipements de Calcul Intensif and particularly those of the High-Performance Computing Platform, which are supported by the FNRS-FRFC, the Walloon Region, and the University of Namur (Conventions No. GEQ U.G006.15, U.G018.19, 1610468, and RW/GEQ2016).

Conflicts of Interest: The authors declare no conflict of interest. The funders had no role in the design of the study, in the collection, analyses, or interpretation of data, in the writing of the manuscript, or in the decision to publish the results.

References

1. Pope, M.T.; Müller, A. Polyoxometalate Chemistry: An Old Field with New Dimensions in Several Disciplines. *Angew. Chem. Int. Ed. Engl.* **1991**, *30*, 34–48. [CrossRef]
2. Anyushin, A.V.; Kondinski, A.; Parac-Vogt, T.N. Hybrid Polyoxometalates as Post-functionalization Platforms: From Fundamentals to Emerging Applications. *Chem. Soc. Rev.* **2020**, *49*, 382–432. [CrossRef]
3. Al-Yasari, A.; Van Steerteghem, N.; El Moll, H.; Clays, K.; Fielden, J. Donor—Acceptor Organo-Imido Polyoxometalates: High Transparency, High Activity Redox-Active NLO Chromophores. *Dalton Trans.* **2016**, *45*, 2818–2822. [CrossRef]
4. Al-Yasari, A.; Van Steerteghem, N.; Kearns, H.; El Moll, H.; Faulds, K.; Wright, J.A.; Brunschwig, B.S.; Clays, K.; Fielden, J. Organoimido-Polyoxometalate Nonlinear Optical Chromophores: A Structural, Spectroscopic, and Computational Study. *Inorg. Chem.* **2017**, *56*, 10181–10194. [CrossRef]
5. Al-Yasari, A.; Spence, P.; El Moll, H.; Van Steerteghem, N.; Horton, P.N.; Brunschwig, B.S.; Fielden, J. Fine-Tuning Polyoxometalate Non-Linear Optical Chromophores: A Molecular Electronic "Goldilocks" Effect. *Dalton Trans.* **2018**, *47*, 10415–10419. [CrossRef] [PubMed]
6. Al-Yasari, A.; El Moll, H.; Purdy, R.; Vincent, B.K.; Spence, P.; Malval, J.P.; Fielden, J. Optical Third Order Non-Linear Optical And Electrochemical Properties Of Dipolar, Centrosymmetric and C2v Organoimido Polyoxometalate Derivatives. *Phys. Chem. Chem. Phys.* **2021**, *23*, 11807–11817. [CrossRef]
7. Boulmier, A.; Vacher, A.; Zang, D.; Yang, S.; Saad, A.; Marrot, J.; Oms, O.; Mialane, P.; Ledoux, I.; Ruhlmann, L.; et al. Anderson-Type Polyoxometalates Functionalized by Tetrathiafulvalene Groups: Synthesis, Electrochemical Studies, and NLO Properties. *Inorg. Chem.* **2018**, *57*, 3742–3752. [CrossRef]
8. Perez-Moreno, J.; Zhao, Y.; Clays, K.; Kuzyk, M.G.; Shen, Y.; Qiu, L.; Hao, J.; Guo, K. Modulated Conjugation as a Means of Improving the Intrinsic Hyperpolarizability. *J. Am. Chem. Soc.* **2009**, *131*, 5084–5093. [CrossRef]
9. Castet, F.; Rodriguez, V.; Pozzo, J.L.; Ducasse, L.; Plaquet, A.; Champagne, B. Design and Characterization of Molecular Nonlinear Optical Switches. *Acc. Chem. Res.* **2013**, *46*, 2656–2665. [CrossRef] [PubMed]
10. Karamanis, P.; Otero, N.; Pouchan, C. Unleashing the Quadratic Nonlinear Optical Responses of Graphene by Confining White-Graphene (h-BN) Sections in Its Framework. *J. Am. Chem. Soc.* **2014**, *136*, 7464–7473. [CrossRef] [PubMed]
11. Nayak, A.; Park, J.; De Mey, K.; Hu, X.; Duncan, T.V.; Beratan, D.N.; Therien, M.J. Large Hyperpolarizabilities at Telecommunication-Relevant Wavelengths in Donor-Acceptor-Donor Nonlinear Optical Chromophores. *ACS Cent. Sci.* **2016**, *2*, 954–966. [CrossRef]
12. Coe, B.J.; Rusanova, D.; Joshi, V.D.; Sanchez, S.; Vavra, J.; Khobragade, D.; Severa, L.; Cisarova, I.; Saman, D.; Pohl, R.; et al. Helquat Dyes: Helicene-like Push−Pull Systems with Large Second-Order Nonlinear Optical Responses. *J. Org. Chem.* **2016**, *81*, 1912–1920. [CrossRef]
13. Lacroix, P.G.; Malfant, I.; Lepetit, C. Second-Order Nonlinear Optics in Coordination Chemistry: An Open Door towards Multi-Functional Materials and Molecular Switches. *Coord. Chem. Rev.* **2016**, *308*, 381–394. [CrossRef]
14. Knoppe, S.; Hakkinen, H.; Verbiest, T.; Clays, K. Role of Donor and Acceptor Substituents on the Nonlinear Optical Properties of Gold Nanoclusters. *J. Phys. Chem. C* **2018**, *122*, 4019–4028. [CrossRef]
15. Van Bezouw, S.; Koo, M.J.; Lee, S.C.; Lee, S.H.; Campo, J.; Kwon, O.P.; Wenseleers, W. Three-Stage pH-Switchable Organic Chromophores with Large Nonlinear Optical Responses and Switching Contrasts. *Chem. Commun.* **2018**, *54*, 7842–7845. [CrossRef]

16. Tonnelé, C.; Champagne, B.; Muccioli, L.; Castet, F. Second-Order Nonlinear Optical Properties of Stenhouse Photoswitches: Insights from Density Functional Theory. *Phys. Chem. Chem. Phys.* **2018**, *20*, 27658–27667. [CrossRef] [PubMed]
17. Lou, A.J.T.; Marks, T.J.A. Twist on Nonlinear Optics: Understanding the Unique Response of π-Twisted Chromophores. *Acc. Chem. Res.* **2019**, *52*, 1428–1438. [CrossRef] [PubMed]
18. Rigamonti, L.; Forni, A.; Cariati, E.; Malavasi, G.; Pasini, A. Solid-State Nonlinear Optical Properties of Mononuclear Copper (II) Complexes with Chiral Tridentate and Tetradentate Schiff Base Ligands. *Materials* **2019**, *12*, 3595. [CrossRef]
19. Rothe, C.; Neusser, D.; Hoppe, N.; Dirnberger, K.; Vogel, W.; Gámez-Valenzuela, S.; Ludwigs, S. Push-Pull Chromophores for Electro-Optic Applications: From 1D Linear to β-branched Structures. *Phys. Chem. Chem. Phys.* **2020**, *22*, 2283–2294. [CrossRef]
20. Qiu, S.; Morshedi, M.; Kodikara, M.S.; Du, J.; de Coene, Y.; Zhang, C.; Humphrey, M.G. Organometallic complexes for nonlinear optics. 66. Synthesis and quadratic nonlinear optical studies of trans-[Ru{C C {2, 5-C4H2S-(E)-CHCH} n-2, 5-C4H2S (NO2)} Cl (dppe) 2](*n* = 0–2). *J. Organomet. Chem.* **2020**, *919*, 121306. [CrossRef]
21. Cesaretti, A.; Foggi, P.; Fortuna, C.G.; Elisei, F.; Spalletti, A.; Carlotti, B. Uncovering Structure—Property Relationships in Push–Pull Chromophores: A Promising Route to Large Hyperpolarizability and Two-Photon Absorption. *J. Phys. Chem.* **2020**, *124*, 15739–15748. [CrossRef]
22. Ramos, T.N.; Canuto, S.; Champagne, B. Unraveling the Electric Field-Induced Second Harmonic Generation Responses of Stilbazolium Ion Pairs Complexes in Solution Using a Multiscale Simulation Method. *J. Chem. Inf. Model.* **2020**, *60*, 4817–4826. [CrossRef] [PubMed]
23. Idney, B.; Tertius, L.F.; Leandro, R.F.; Herbert, C.G.; Marcos, A.C. Applicability of DFT Functionals for Evaluating the First Hyperpolarizability of Phenol Blue in Solution. *J. Chem. Phys.* **2021**, *154*, 094501. [CrossRef]
24. Moris, M.; Van Den Eede, M.P.; Koeckelberghs, G.; Deshaume, O.; Bartic, C.; Clays, K.; Cleuvenbergen, S.; Verbiest, T. Solvent Role in the Self-Assembly of Poly (3-alkylthiophene): A Harmonic Light Scattering Study. *Macromolecules* **2021**, *54*, 2477–2484. [CrossRef]
25. Castet, F.; Gillet, A.; Bureš, F.; Plaquet, A.; Rodriguez, V.; Champagne, B. Second-Order Nonlinear Optical Properties of Λ-Shaped Pyrazine Derivatives. *Dye. Pigment.* **2021**, *184*, 108850. [CrossRef]
26. Verbiest, T.; Clays, K.; Rodriguez, V. *Second-Order Nonlinear Optical Characterizations Techniques: An Introduction*; CRC Press: New York, NY, USA, 2009.
27. Yan, L.; Yang, G.; Guan, W.; Su, Z.; Wang, R. Density Functional Theory Study on the First Hyperpolarizabilities of Organoimido Derivatives of Hexamolybdates. *J. Phys. Chem. B* **2005**, *109*, 22332–22336. [CrossRef]
28. Janjua, M.R.S.A.; Liu, C.G.; Guan, W.; Zhuang, J.; Muhammad, S.; Yan, L.K.; Su, Z.M. Prediction of Remarkably Large Second-Order Nonlinear Optical Properties of Organoimido-Substituted Hexamolybdates. *J. Phys. Chem.* **2009**, *113*, 3576–3587. [CrossRef]
29. Rtibi, E.; Abderrabba, M.; Ayadi, S.; Champagne, B. Theoretical Assessment of the Second-Order Nonlinear Optical Responses of Lindqvist-Type Organoimido Polyoxometalates. *Inorg. Chem.* **2019**, *58*, 11210–11219. [CrossRef]
30. Lescos, L.; Sitkiewicz, S.; Beaujean, P.; Blanchard-Desce, M.; Champagne, B.; Matito, R.E.; Castet, F. Performance of DFT Functionals for Calculating the Second-Order Nonlinear Optical Properties of Dipolar Merocyanines. *Phys. Chem. Chem. Phys.* **2020**, *22*, 16579–16594. [CrossRef]
31. Champagne, B.; Perpète, E.A.; Jacquemin, D.; van Gisbergen, S.J.A.; Baerends, E.J.; Soubra-Ghaoui, C.; Kirtman, B. Assessment of Conventional Density Functional Schemes for Computing the Dipole Moment and (Hyper)polarizabilities of Push–Pull π-Conjugated Systems. *J. Phys. Chem.* **2000**, *104*, 4755–4763. [CrossRef]
32. Bulat, F.A.; Toro-Labbé, A.; Champagne, B.; Kirtman, B.; Yang, W. Density-Functional Theory (hyper) polarizabilities of Push-Pull π-Conjugated Systems: Treatment of Exact Exchange and Role of Correlation. *J. Chem. Phys.* **2005**, *123*, 014319. [CrossRef] [PubMed]
33. Sun, H.; Autschbach, J. Influence of the Delocalization Error and Applicability of Optimal Functional Tuning in Density Functional Calculations of Nonlinear Optical Properties of Organic Donor-Acceptor Chromophores. *ChemPhysChem* **2013**, *14*, 2450–2461. [CrossRef] [PubMed]
34. Frisch, M.J.; Trucks, G.W.; Schlegel, H.B.; Scuseria, G.E.; Robb, M.A.; Cheeseman, J.R.; Scalmani, G.; Barone, V.; Petersson, G.A.; Nakatsuji, H.; et al. *Gaussian 16, Revis. C.01*; Gaussian Inc.: Wallingford, CT, USA, 2016.
35. Chai, J.D.; Head-Gordon, M. Long-range Corrected Hybrid Density Functionals with Damped Atom-Atom Dispersion Corrections. *Phys. Chem. Chem. Phys.* **2008**, *10*, 6615–6620. [CrossRef] [PubMed]
36. Becke, A.D. Density-Functional Thermochemistry. V. Systematic Optimization of Exchange-Correlation Functionals. *J. Chem. Phys.* **1997**, *107*, 8554–8560. [CrossRef]
37. Tomasi, J.; Mennucci, B.; Cammi, R. Quantum Mechanical Continuum Solvation Models. *Chem. Rev.* **2005**, *105*, 2999–3094. [CrossRef]
38. Van Gisbergen, S.J.A.; Snijders, J.G.; Baerends, E.J. Calculating Frequency-Dependent Hyperpolarizabilities Using Time-Dependent Density Functional Theory. *J. Chem. Phys.* **1998**, *109*, 10644–10656. [CrossRef]
39. Helgaker, T.; Coriani, S.; Jørgensen, P.; Kristensen, K.; Olsen, J.; Ruud, K. Recent Advances in Wave Function-Based Methods of Molecular-Property Calculations. *Chem. Rev.* **2012**, *112*, 543–631. [CrossRef]
40. Bersohn, R.; Pao, Y.H.; Frisch, H.L. Double-Quantum Light Scattering by Molecules. *J. Chem. Phys.* **1966**, *45*, 3184–3198. [CrossRef]
41. Castet, F.; Bogdan, E.; Plaquet, A.; Ducasse, L.; Champagne, B.; Rodriguez, V. Reference Molecules for Nonlinear Optics: A Joint Experimental and Theoretical Investigation. *J. Chem. Phys.* **2012**, *136*, 024506. [CrossRef]

42. Tuer, A.; Krouglov, S.; Cisek, R.; Tokarz, D.; Barzda, V. Three-Dimensional Visualization of the First Hyperpolarizability Tensor. *J. Comput. Chem.* **2011**, *32*, 1128–1134. [CrossRef]
43. Orr, B.J.; Ward, J.F. Perturbation Theory of the Non-Linear Optical Polarization of an Isolated System. *Mol. Phys.* **1971**, *20*, 513–526. [CrossRef]
44. Bishop, D.M. Explicit Non-divergent Formulas for Atomic and Molecular Dynamic Hyperpolarizabilities. *J. Chem. Phys.* **1994**, *100*, 6535–6542. [CrossRef]
45. Oudar, J.L.; Chemla, D.S. Hyperpolarizabilities of the Nitroanilines and Their Relations to the Excited State Dipole Moment. *J. Chem. Phys.* **1977**, *66*, 2664–2668. [CrossRef]
46. Zutterman, F.; Liégeois, V.; Champagne, B. Simulation of UV/visible Absorption Spectra of Fluorescent Protein Chromophore Models. *ChemPhotoChem* **2017**, *1*, 281–297. [CrossRef]
47. Champagne, B.; Kirtman, B. Alternative Sum-Over-States Expressions for the First Hyperpolarizability of Push-Pull π-Conjugated Systems. *J. Chem. Phys.* **2006**, *125*, 024101. [CrossRef]
48. Wei, Y.; Lu, M.; Cheung, C.F.-C.; Barnes, C.L.; Peng, Z. Functionalization of $[MoW_5O_{19}]^{2-}$ with Aromatic Amines: Synthesis of the First Arylimido Derivatives of Mixed-Metal Polyoxometalates. *Inorg. Chem.* **2001**, *40*, 5489–5490. [CrossRef]